Seventh International Conference on Computational Fluid Dynamics (ICCFD7), Big Island, Hawaii, July 9-13, 2012

ICCFD7-2606

Robust performance assessment for an oscillating airfoil combining the Time Spectral Method and a semi-intrusive uncertainty propagation approach

P.M. Congedo*, C. Corre** and R. Abgrall*
Corresponding author: Christophe.Corre@legi.grenoble-inp.fr

* Team Bacchus, INRIA Bordeaux Sud Ouest
** Grenoble-INP/UJF Grenoble/CNRS LEGI UMR5519, Grenoble, France.

Abstract: The power extracted from a flowing fluid by an oscillating airfoil in a combined heaving and pitching motion is analyzed with fluctuations of the heaving amplitude taken into account. The uncertainties on the airfoil motion are propagated throughout the ALE artificial compressibility solver using an original semi-intrusive (SI) method which can be applied to uncertainties described by any type of probability density function.The computational cost is reduced thanks to an implicit time spectral (TSM) method. The TSM / SI strategy is compared, in terms of accuracy and robustness, with a more conventional dual-time-step / non-intrusive polynomial chaos approach.

Keywords: uncertainty propagation, semi-intrusive strategy, Time Spectral Method, oscillating airfoil, uncertain motion

1 Introduction

The energy that may be extracted from an incoming flow by a heaving and pitching airfoil has been numerically quantified by Kinsey and Dumas [1]. These authors performed a parametric study of the airfoil performance using a dual-time-step (DTS) method for describing the unsteady flow evolution and identified the frequency and pitching-amplitude maximizing the amount of power extracted for a fixed heaving amplitude. Though somewhat limited in its scope (single airfoil, laminar-flow conditions) this study provides useful guidelines for designing actual power-extraction systems. The optimal operating point in the pitching frequency/amplitude space identified in Kinsey and Dumas study was obtained by assuming perfectly fixed values of the parameters describing the airfoil motion (heaving and pitching amplitudes, frequency). In practice, these parameters are subject to fluctuations and should rather be described as stochastic variables with their associated probability density functions. Consequently, the computed power or efficiency of the energy-extracting device is no longer given by a single deterministic value but described by statistical moments. A robust design will take into account at least the expectation and the variance of the quantity of interest, say the global efficiency of the device. In order to compute such moments on output quantities, the uncertainty on the design variables (here the airfoil motion parameters) must be propagated through the simulation. The Monte Carlo method (MCM) is a popular approach to model uncertainty because of its versatility but remains in general too expensive to be considered in CFD stochastic computations; in fact MCM may become competitive when a very high-dimension probability space is considered since its order of convergence does not depend on the number of random parameters. Several stochastic methods are based on dividing the probability space into multiple subdomains and using a polynomial approximation of the response surface [2] [3]. Other approaches are the intrusive [4] [5] [6] [7] and non-intrusive [8] [9] [10] formulations relying on Polynomial Chaos expansion of the random variables. Polynomial Chaos methods, first introduced by

Ghanem and Spanos [4] appear to be a good alternative to statistical methods for uncertainty quantification. In 2002, Xiu and Karniadakis introduced Generalized Polynomial Chaos [5]; it was demonstrated the type of orthogonal polynomials in the chaos expansion should correspond to the properties of the stochastic process based on the association between probability density functions (pdf) and weighting functions in order to achieve optimal convergence. Wan and Karniadakis have developed in [11] a multi-element polynomial chaos method : the space of random input is adaptively decomposed into multiple elements and polynomial chaos expansions are used at the element level. An important requirement to comply with is the versatility of the UQ method that should allow to deal with any form of pdf that might arise for instance from a set of experiments. In the case of non-intrusive methods, the input random space can be sampled by very specific random events that are associated to the Gaussian points of the integration formulation corresponding to the expectancy. Thus, it is possible to consider *a priori* any type of pdf providing these quadrature points are evaluated. In practice however an orthogonal (with respect to the pdf) polynomial basis has to be computed and the zeros of the highest degree polynomial must be found with a great accuracy, a difficult task in many circumstances. A new so-called semi-intrusive (SI) approach, particularly suited for flow problems and offering flexibility with respect to the form of the pdf, has been proposed in [12] and applied to steady and unsteady $1D$ compressible flow problems in [13]. This SI approach will be extended in the present work to deal with $2D$ incompressible unsteady flows over an oscillating airfoil whose motion is not known with certainty.

As far as the computational cost is concerned, the overall cost of a UQ method, be it intrusive or not, is directly dependent on the efficiency of the baseline deterministic solver. For the time-periodic flow of interest in this study this efficiency can be significantly increased by using a Time-Spectral Method (TSM) instead of a conventional time-marching strategy such as a second-order implicit Backward Difference Formula (BDF). When applied to a d-dimensional compressible flow field, the TSM approach transforms the original system of $(d+2)$ unsteady governing equations into the solution of $(2N+1) \times (d+2)$ coupled steady equations corresponding to the flow solution at $(2N+1)$ time moments in the flow period, selected so as to ensure spectral accuracy for the physical time-derivative. While well developed for compressible flows [14]-[20], the TSM approach has only been recently extended to incompressible flows using a finite-volume formulation of the Artificial Compressibility system on general moving unstructured grids [21]. The oscillating airfoil configuration studied by Kinsey and Dumas was then computed with a conventional time-marching approach describing the whole transient behavior and the proposed implicit TSM approach; it was demonstrated that TSM could afford a substantial cost reduction (up to a factor of 5) with respect to standard unsteady solution techniques.

The resolution of the pitching and heaving airfoil problem with uncertain motion will take advantage of TSM efficiency, both when coupling in a straightforward manner the deterministic solver with a non-intrusive polynomial chaos (NIPC) strategy and when implementing in the CFD solver the semi-intrusive UQ strategy proposed in [12]. The NIPC approach will rely on the NISP (Non Intrusive Spectral Projection) toolbox developed by Jean-Marc Martinez and Michael Baudin in the framework of the ANR Opus Project [22] [23].

The paper is organized as follows : the physical problem under consideration is described in Section 2 so as to clarify the numerical requirements associated with the solution of this stochastic problem. The available deterministic CFD solver is briefly described in Section 3, both in its implicit time-marching and TSM formulation; a brief comparison of the methods for the oscillating airfoil problem is presented. The theoretical principles and practical implementation of the non-intrusive and semi-intrusive UQ strategies used in this work are presented in Section 4; computational details on the SI approach are provided so as to make clear how the existing BDF or TSM CFD solver has to be only slightly modified in order to be extended to the computation of flows involving uncertain parameters described by any type of pdf; some key preliminary results obtained for the oscillating airfoil problem with uncertain motion are analyzed. Short-term perspectives are outlined in the conclusion of the paper.

2 Description of the physical problem

The geometry under study is a NACA0015 airfoil submitted to a pitching motion and a heaving motion. These prescribed motions are defined by the following laws of evolution for the pitching angle $\theta(t)$ around

an axis located at one-third of the airfoil chord and the vertical position $y(t)$:

$$\begin{cases} \theta(t) = \theta_0 \, sin(\omega t) \\ y(t) = H_0 \, sin(\omega t + \pi/2) \end{cases} \tag{1}$$

where θ_0 and H_0 are respectively the pitching and heaving amplitudes, ω is the angular velocity. The reduced frequency f^* is defined as $f^* = fc/U_\infty$with c the airfoil chord and U_∞ the free stream velocity. The reference test case in the present study corresponds to a combination of pitching and heaving motion with $\theta_0 = 60°$, $H_0 = 1$ and $f^* = 0.18$; it will be denoted PH from now on. The Reynolds number based on the upstream uniform velocity U_∞ and the airfoil chord is equal to 1100 so that the flow can be considered laminar. Let us assume the heaving amplitude H_0 cannot be rigorously prescribed to be equal to unity in practice : for instance, the mechanism actually used to impose the airfoil motion yields values of H_0 which fluctuate randomly within some minimum (H_0^{min}) and maximum (H_0^{max}) bounds. Both for lack of actual experimental data and for the sake of demonstrating the potential of the SI approach in a case where the NIPC approach can be applied so as to allow comparisons between SI and NIPC, it is assumed the fluctuations of H_0 can be described by a uniform pdf over the interval $[H_0^{min}, H_0^{max}]$. Since the efficiency of the power-extracting device directly derives from the evolution of the horizontal and vertical aerodynamic force coefficients C_X, C_Y over a cycle of the periodic motion, the analysis will be focused on computing the statistical moments of these quantities of interest. Typically we are looking for the mean value $\overline{C}_X$ or $\overline{C}_Y$ and the variance $\sigma(C_X)$ or $\sigma(C_Y)$ of the aerodynamic force coefficients at each time-instance over a flow period. Whatever the strategy retained for propagating the motion uncertainty throughout the simulation, the starting point remains in any case a deterministic flow solver allowing to compute the unsteady flow over the airfoil for a fixed value of H_0. The baseline solver used in the present study is described in the next Section both in its standard time-marching version and its original time spectral formulation.

3 CFD deterministic solver

3.1 General principles

The flow over the airfoil is described by the 2D incompressible Navier-Stokes equations. The solution of the incompressible Navier-Stokes equations is typically obtained using either a pressure-based method where pressure and velocity are solved in an iterative fashion through a pressure-correction equation, or a density-based method, such as the artificial compressibility (AC) approach of Chorin [24] The latter AC strategy has been favored in this work to take advantage of efficient implicit methods previously developed for solving hyperbolic problems [27] and easy to adapt to the AC system. Let us recall the AC method provides a time-accurate solution of the 1D Euler equations by finding the steady-state of the following hyperbolic system of conservation laws with respect to the dual or fictitious time τ :

$$\frac{\partial}{\partial \tau} \underbrace{\begin{pmatrix} p \\ u \end{pmatrix}}_{=\mathbf{w}} + \underbrace{\begin{pmatrix} 0 & 0 \\ 0 & 1 \end{pmatrix}}_{=\mathbf{K}} \cdot \frac{\partial}{\partial t} \begin{pmatrix} p \\ u \end{pmatrix} + \underbrace{\frac{\partial}{\partial x} \begin{pmatrix} \beta u \\ u^2 + p \end{pmatrix}}_{=\mathbf{f}(\mathbf{w};\beta)} \tag{2}$$

with x the space variable, t the physical time, p, u the pressure and velocity, β the constant artificial compressibility parameter. At steady-state on τ, the solution $u(x,t)$ of (2) satisfies the zero-divergence condition while both fields $u(x,t)$ and $p(x,t)$ satisfy the unsteady (with respect to t) momentum equation. Rewriting (2) in the compact form of a 1D hyperbolic system with a source term :

$$\frac{\partial \mathbf{w}}{\partial \tau} + \frac{\partial}{\partial x} \mathbf{f}(\mathbf{w};\beta) = \mathbf{S} = -\mathbf{K} \frac{\partial \mathbf{w}}{\partial t}$$

makes clear the AC system can be efficiently driven to an accurate steady-solution by making use of tools initially developed in the context of compressible flow solutions: second-order upwind discretization for the flux derivative, second-order Backward Difference Formula (BDF) discretization for the physical time-derivative and first-order implicit stage for fast convergence on the dual-time. Note the choice of value for the AC parameter β affects the overall convergence rate as well as the accuracy of the physical solution

through the numerical dissipation of the space discretization; however, as long as the steady-state on τ is correctly achieved, the AC system remains consistent with the incompressible flow equations whatever the value of β. Let us now turn to the AC system extended to the case of incompressible viscous flows computed on moving grids. Let $C(t)$ be an arbitrary control volume bounded by a smooth closed surface $\partial C(t)$, which moves independently from the flow with a velocity $\mathbf{s}(x,t) = s_x(t)\mathbf{i} + s_y(t)\mathbf{j}$, where $\mathbf{x} = x\mathbf{i} + y\mathbf{j}$ denotes the vector of Cartesian coordinates in the absolute frame of reference. In the Arbitrary Lagrangian Eulerian (ALE) framework, the 2D Navier-Stokes equations for incompressible unsteady flows, modified to account for the AC method, can be expressed in the following integral form:

$$\mathbf{K}\frac{\partial}{\partial t}\int_{C(t)} \mathbf{w}(\mathbf{x},t)\, dS + \int_{\partial C(t)} (\mathbf{F}^E - \mathbf{F}^V)\cdot \mathbf{n}\, d\gamma = 0 \tag{3}$$

where $\mathbf{n}$ is the outward unit normal vector to $\partial C(t)$ and γ the curvilinear abscissa along $\partial C(t)$. The vector of conservative variables $\mathbf{w}$, the singular matrix $\mathbf{K}$, the inviscid fluxes $\mathbf{F}^E = (\mathbf{f}^E, \mathbf{g}^E)$ and the viscous fluxes $\mathbf{F}^V = (\mathbf{f}^V, \mathbf{g}^V)$ are defined by :

$$\mathbf{w} = \begin{pmatrix} p \\ u \\ v \end{pmatrix}, \quad \mathbf{K} = \begin{pmatrix} 0 & 0 & 0 \\ 0 & 1 & 0 \\ 0 & 0 & 1 \end{pmatrix}, \quad \mathbf{f}^E(\mathbf{w}) = \begin{pmatrix} \beta(u - s_x) \\ u(u - s_x) + p \\ v(u - s_x) \end{pmatrix}, \quad \mathbf{g}^E(\mathbf{w}) = \begin{pmatrix} \beta(v - s_y) \\ u(v - s_y) \\ v(v - s_y) + p \end{pmatrix}$$

$$\mathbf{f}^V(\frac{\partial \mathbf{w}}{\partial x}, \frac{\partial \mathbf{w}}{\partial y}) = \frac{1}{Re}\begin{pmatrix} 0 \\ 2\dfrac{\partial u}{\partial x} \\ \dfrac{\partial u}{\partial y} + \dfrac{\partial v}{\partial x} \end{pmatrix}, \quad \mathbf{g}^V(\frac{\partial \mathbf{w}}{\partial x}, \frac{\partial \mathbf{w}}{\partial y}) = \frac{1}{Re}\begin{pmatrix} 0 \\ \dfrac{\partial u}{\partial y} + \dfrac{\partial v}{\partial x} \\ 2\dfrac{\partial v}{\partial y} \end{pmatrix}$$

System (3) is solved on general unstructured grids using a finite volume approach. Applying (3) on a given cell C_i, introducing the average value of $\mathbf{w}$ over the cell, decomposing the flux balance as the sum of fluxes through each face $\Gamma_{i,k}$ of cell C_i and using numerical flux formulae to approximate the physical flux through each grid face leads to :

$$\frac{\partial \mathbf{w}_i}{\partial \tau} + \mathbf{K}\frac{\partial \mathbf{w}_i}{\partial t} + \mathcal{R}_i^E(\mathbf{w}, \mathbf{x}, \mathbf{s}) = \mathcal{R}_i^V(\mathbf{w}, \mathbf{x}) \tag{4}$$

The inviscid numerical flux balance or residual is defined by :

$$\mathcal{R}_i^E(\mathbf{w}, \mathbf{x}, \mathbf{s}) = \frac{1}{|C_i|}\sum_k \mathcal{H}_{i,k}^E |\Gamma_{i,k}| \tag{5}$$

where $\mathcal{H}_{i,k}^E$ is the numerical flux approximating the inviscid physical flux through face $\Gamma_{i,k}$. Note that, in the context of the ALE formulation, the dependence of this residual on the mesh position $\mathbf{x}$ and speed $\mathbf{s}$ has been made explicit. Similarly, the viscous flux balance or residual takes the form :

$$\mathcal{R}_i^V(\mathbf{w}, \mathbf{x}) = \frac{1}{|C_i|}\sum_k \mathcal{H}_{i,k}^V |\Gamma_{i,k}| \tag{6}$$

where $\mathcal{H}_{i,k}^V$ is the numerical flux approximating the viscous physical flux through face $\Gamma_{i,k}$. Note the cell surface $|C_i|$ will stay constant over time since the present work will only consider rigid body motion for the grid. The second-order accurate schemes used in the present work are such that :

$$\begin{cases} \mathcal{H}_{i,k}^E = \mathcal{H}^E(\mathbf{w}_i, \nabla \mathbf{w}_i; \mathbf{w}_{o(i,k)}, \nabla \mathbf{w}_{o(i,k)}) \\ \mathcal{H}_{i,k}^V = \mathcal{H}^V(\nabla \mathbf{w}_{N_{i,k}^1}; \nabla \mathbf{w}_{N_{i,k}^2}) \end{cases} \tag{7}$$

The purposely compact notations used in (7) emphasize the dependence of the inviscid numerical flux on the physical states and gradients at the centers of cells i and $o(i,k)$ sharing face $\Gamma_{i,k}$ and the dependence of the viscous numerical flux on the gradients of $\mathbf{w}$ computed at the nodes $N_{i,k}^1$ and $N_{i,k}^2$ of face $\Gamma_{i,k}$. The

inviscid numerical flux formula used in the present work will be of Roe type and the cell-centered states and gradients will be used to compute the face-centered reconstructed states $\mathbf{w}_{i,k}^L$ and $\mathbf{w}_{i,k}^R$ on each side of $\Gamma_{i,k}$ (such that $\mathcal{H}_{i,k}^E = \mathcal{H}^E(\mathbf{w}_{i,k}^L, \mathbf{w}_{i,k}^R)$) :

$$\left\{ \begin{array}{l} \mathbf{w}_{i,k}^L = \mathbf{w}_i + \nabla \mathbf{w}_i \cdot \mathbf{r}_{i,k} \\ \\ \mathbf{w}_{i,k}^R = \mathbf{w}_{o(i,k)} + \nabla \mathbf{w}_{o(i,k)} \cdot \mathbf{r}_{o(i,k),k} \end{array} \right. \tag{8}$$

where $\mathbf{r}_{i,k}$ (respectively $\mathbf{r}_{o(i,k),k}$) denotes the vector joining the center of cell i (resp. $o(i,k)$) to the center of face $\Gamma_{i,k}$. The viscous numerical flux formula is a simply centered approximation of the viscous physical flux formula where the velocity gradients at the face nodes are averaged to estimate the velocity gradient at the face center. The cell-centered and node-centered gradients are computed using least-square approximate on pre-defined stencils (see [25] for more details).

3.2 Conventional BDF time-discretization

When the physical time-derivative in (4) is approximated using the second-order implicit Backward Difference Formula (BDF) the fully discrete form of the AC-ALE system reads :

$$\frac{\mathbf{w}_i^{n,m+1} - \mathbf{w}_i^{n,m}}{\Delta \tau_i^{n,m}} + \mathbf{K} \frac{\left(\frac{3}{2}\mathbf{w}_i^{n,m} - 2\mathbf{w}_i^n + \frac{1}{2}\mathbf{w}_i^{n-1}\right)}{\Delta t} + \mathcal{R}_i(\mathbf{w}^{n,m}) = 0 \tag{9}$$

where $\mathcal{R}_i(\mathbf{w}) = \mathcal{R}_i^E(\mathbf{w}) - \mathcal{R}_i^V(\mathbf{w})$ with the dependence on the grid position and grid velocity in the expressions of $\mathcal{R}_i^E$ and $\mathcal{R}_i^V$ omitted in the formula for the sake of simplicity. The second-order accurate approach followed to take into account the grid motion is derived from [26]; details on the discrete formulae used to compute the grid motion and velocity can be found in [21]. The global efficiency of the approach is ensured by making use of an implicit (with respect to the dual time τ) solution strategy for (9), taking advantage of previously developed low-cost implicit methods dedicated to steady-flow computations such as the matrix-free implicit solver described in [27]. In order to simplify the description of the method, lets us introduce the following notations :

$$\mathcal{T}(\mathbf{w}_i^{n,m}, \mathbf{w}_i^n, \mathbf{w}_i^{n-1}) = \frac{\left(\frac{3}{2}\mathbf{w}_i^{n,m} - 2\mathbf{w}_i^n + \frac{1}{2}\mathbf{w}_i^{n-1}\right)}{\Delta t} \quad , \quad \mathcal{R}_i^t(\mathbf{w}^{n,m}) = \mathbf{K}\mathcal{T}(\mathbf{w}_i^{n,m}, \mathbf{w}_i^n, \mathbf{w}_i^{n-1}) + \mathcal{R}_i(\mathbf{w}^{n,m})$$

Making the scheme implicit with respect to τ requires to solve the non-linear system of equations :

$$\Delta \mathbf{w}_i^{n,m} = -\Delta \tau_i^{n,m} \, \mathcal{R}_i^t(\mathbf{w}^{n,m+1})$$

where $\Delta \mathbf{w}_i^{n,m} = \mathbf{w}_i^{n,m+1} - \mathbf{w}_i^{n,m}$. The total residual, including the physical time derivative, is approximately expanded as :

$$\mathcal{R}_i^t(\mathbf{w}^{n,m+1}) \approx \mathcal{R}_i^t(\mathbf{w}^{n,m}) + \frac{3}{2}\frac{\mathbf{K}}{\Delta t}\Delta \mathbf{w}_i^{n,m} + \mathcal{I}(\Delta \mathbf{w}^{n,m})$$

with $\mathcal{I}(\Delta \mathbf{w}^{n,m})$ a simplified estimate of $\left(\frac{d\mathcal{R}_i}{d\mathbf{w}}\right)^{n,m} \Delta \mathbf{w}^{n,m}$. Owing to the respective definitions (5) and (6) of the inviscid and viscous residual, computing this simplified estimate of the residual requires to approximate the Jacobian of the numerical fluxes $\frac{d\mathcal{H}^E}{d\mathbf{w}}$ and $\frac{d\mathcal{H}^V}{d\mathbf{w}}$. A possible choice, detailed in [27], is to make use of simplified numerical flux formulae in the implicit stage yielding easy to compute flux Jacobian. The resulting

solution method takes the form :

$$\begin{array}{l} \Delta \mathbf{w}_i^{(0)} = 0 \\ \left\{ \begin{array}{l} l = 0, l_{max} - 1 \\ \Delta \mathbf{w}_i^{(l+1)} = (\mathbf{D}_i^{n,m})^{-1} \left(-\Delta \tau_i^{n,m} \mathcal{R}_i^t(\mathbf{w}^{n,m}) - \dfrac{\Delta \tau_i^{n,m}}{2|C_i|} \displaystyle\sum_k \left(\Delta \mathbf{F}^E_{o(i,k)} \right)^{(l)} \cdot \mathbf{n}_{i,k} |\Gamma_{i,k}| + \sum_k C_{i,k}^{n,m} \Delta \mathbf{w}^{(l)}_{o(i,k)} \right) \end{array} \right. \\ \mathbf{w}_i^{n,m+1} = \mathbf{w}_i^{n,m} + \Delta \mathbf{w}_i^{(l_{max})} \end{array} \tag{10}$$

where $\Delta \phi^{(l)} = \phi^{(l)} - \phi^{n,m}$ and the matrix $\mathbf{D}_i^{n,m}$ and scalars $C_{i,k}^{n,m}$ are defined as :

$$\mathbf{D}_i^{n,m} = \left(\mathbf{I} + \frac{3}{2} \frac{\Delta \tau_i^{n,m}}{\Delta t} \mathbf{K} + \sum_k C_{i,k}^{n,m} \mathbf{I} \right) \quad , \quad C_{i,k}^{n,m} = \frac{\Delta \tau_i^{n,m} |\Gamma_{i,k}|}{|C_i|} \left(\frac{1}{2} \rho(\mathbf{J}_\perp^E) + \rho(\widetilde{\mathbf{J}_\perp^V}) \right)_{i,k}^{n,m} \tag{11}$$

The matrices $\mathbf{J}_\perp^E$ and $\mathbf{J}_\perp^V$ denote respectively the Jacobian of the inviscid and viscous normal flux to the face $\Gamma_{i,k}$ and $\rho(\mathbf{M})$ is the spectral radius of the matrix $\mathbf{M}$. The quantity $\rho(\widetilde{\mathbf{J}_\perp^V})$ corresponds to $\rho(J_\perp^V)/(||\mathbf{r}_{i,k}|| + ||\mathbf{r}_{o(i,k),k}||)$. From now on, the solution method described by (10) will be referred to as PJ-BDF-ALE-AC where PJ stands for Point Jacobi, the relaxation technique used to solve the simplified implicit stage.

3.3 Time Spectral Method

When computing an unsteady flow of period T, one can take advantage of the time periodicity of $\mathbf{w}$ in order to decompose the solution vector into a Fourier series :

$$\mathbf{w} = \sum_{k=-\infty}^{+\infty} \widehat{\mathbf{w}_k}(x) e^{\underline{i} k \omega t} \tag{12}$$

where ω is the pulsation of the periodic phenomenon related to the period T by $\omega = 2\pi/T$. The complex number $\underline{i}$ is underlined to avoid confusion with the cell index i. In practice, the solution is represented with a finite number of harmonics N :

$$\mathbf{w} = \sum_{k=-N}^{N} \widehat{\mathbf{w}_k}(x) e^{\underline{i} k \omega t} \tag{13}$$

The Nyquist-Shannon theorem states that the k^{th} Fourier coefficient $\widehat{\mathbf{w}_k}$ with $-N \leq k \leq N$ can be accurately computed with $2N+1$ time instances evenly distributed over the time period :

$$\widehat{\mathbf{w}_k}(x) = \frac{1}{2N+1} \sum_{n=0}^{2N} \mathbf{w}_n e^{-\underline{i} k \omega n \Delta t} \tag{14}$$

with $\mathbf{w}_n \equiv \mathbf{w}(t_n = n\Delta t)$ and $\Delta t = T/(2N+1)$. The main idea of the TSM method is to look for these modes $\mathbf{w}_n$ in order to retrieve the solution at any time t in the period using (13). The space-discretized ALE-AC system at time instance t_n reads :

$$\mathbf{K} \frac{\mathbf{w}_n}{\partial t} + \mathcal{R}(\mathbf{w}_n, \mathbf{s}_n, \mathbf{x}_n) = 0 \tag{15}$$

where $\mathbf{w} = \{\mathbf{w}_i\}$ is the set of solution values in all the grid cells and $\mathcal{R} = \{\mathcal{R}_i\}$ is the set of residual values computed in all the grid cells, which depends non-linearly on $\mathbf{w}$. From now on, $\mathbf{w}_{i,n}$ will denote the solution at grid point i and at time instance t_n in the flow period. Using the Fourier decomposition (13) into equation

(15) leads to $2N+1$ equations (one for each wavenumber) in the frequency domain :

$$\mathbf{K} \underbrace{\sum_{k=-N}^{N} \underline{i}k\omega\widehat{\mathbf{w}_k}e^{ik\omega n\Delta t}}_{=D_t(\mathbf{w}_n)} + \hat{\mathcal{R}}(\widehat{\mathbf{w}_k}, \widehat{\mathbf{x}_k}, \widehat{\mathbf{s}_k}) = 0 \tag{16}$$

where $D_t(\mathbf{w}_n)$ is the spectral derivative with respect to time which couples the wavenumbers. The operator $\hat{\mathcal{R}}$ could be directly computed from $\widehat{\mathbf{w}_k}$ but, because of its non-linearity, this would involve complex series of convolution becoming massively time consuming. Using (14) allows to cast system (16) back into the time domain and to retrieve the original residual vector $\mathcal{R}$ because of the biobjective property of the Fourier transform :

$$\mathbf{K}D_t(\mathbf{w}_n) + \mathcal{R}(\mathbf{w}_n, \mathbf{x}_n, \mathbf{s}_n) = 0 \tag{17}$$

where the spectral time operator expressed in the time domain becomes :

$$D_t(\mathbf{w}_n) = \sum_{p=-N}^{N} d_p \mathbf{w}_{n+p} \tag{18}$$

with the d_p coefficients given by :

$$d_p = \begin{cases} \dfrac{\pi}{T}(-1)^{(p+1)} cot\left(\dfrac{\pi p}{N}\right) & \text{if } p \neq 0 \\ 0 & \text{if } p = 0 \end{cases} \tag{19}$$

and where the subscript $n+p$ in (18) refers to the remainder of the euclidian division of $n+p$ by $2N+1$. Since the spectral time-derivative depends on the whole set of solutions $\mathbf{w}_{n+p}$ with p ranging from $-N$ to N, system (17) must be written for each time instance in the period :

$$\mathbf{K}D_t(\mathbf{w}_n) + \mathcal{R}(\mathbf{w}_n, \mathbf{x}_n, \mathbf{s}_n) = 0, \qquad 0 \leq n < 2N+1 \tag{20}$$

This non-linear system of equations is iteratively solved through a dual time-marching strategy, that is looking for the steady state with respect to τ of the following system :

$$\frac{\partial \mathbf{w}_n}{\partial \tau} = -\mathcal{R}_n^t(\mathbf{w}), \qquad 0 \leq n < 2N+1 \tag{21}$$

where the total residual is defined as $\mathcal{R}_n^t(\mathbf{w}) = \mathbf{K}D_t(\mathbf{w}_n) + \mathcal{R}(\mathbf{w}_n, \mathbf{x}_n, \mathbf{s}_n)$ for the TSM approach. The $2N+1$ sets of steady values $\mathbf{w}_n$ are coupled through the spectral approximation $D_t(\mathbf{w}_n)$ of the physical time derivative. Let us denote $\mathbf{w}_n^m$ the intermediate value of $\mathbf{w}_n$ at the m^{th} iteration of the dual-time evolution to a steady-state. Using an Euler implicit discretization for the dual-time derivative, the steady-state is reached by iteratively solving the following system in each cell of the computational grid at time instance t_n within the period :

$$\Delta \mathbf{w}_{i,n}^m = -\Delta\tau_{i,n}^m \, \mathcal{R}_{i,n}^t(\mathbf{w}^{m+1}, \mathbf{x}_n, \mathbf{s}_n), \qquad 0 \leq n < 2N+1 \tag{22}$$

where $\Delta \mathbf{w}_n^m = \mathbf{w}_n^{m+1} - \mathbf{w}_n^m$ and $\Delta\tau_{i,n}^m$ is the local (dual) time-step. Note that, in the present study, the $2N+1$ grid positions and velocities are *a priori* known from the prescribed grid motion when a fully deterministic computation is performed while these quantities will depend on the uncertain parameter H_0 when performing the stochastic analysis. Following a line of work similar to that described for the BDF approach, the TSM residual at dual time-level $m+1$ can be approximately expanded as follows :

$$\mathcal{R}_{i,n}^t(\mathbf{w}^{m+1}) \approx \mathcal{R}_{i,n}^t(\Delta\mathbf{w}^m) + \mathbf{K}D_t(\Delta\mathbf{w}_{i,n}^m) + \frac{1}{|C_i|}\sum_k \left(\Delta\mathcal{H}_{(i,k),n}^{(imp)}\right)^m |\Gamma_{i,k}|$$

where the flux increment balance $\Delta\mathcal{H}^{(i)}$ is computed using the same simplified formulae for the inviscid and viscous numerical fluxes than the ones previously used when deriving the BDF implicit stage - with the

variable increment $\Delta \mathbf{w}_{i,n}^m$ replacing $\Delta \mathbf{w}_i^{n,m}$. The resulting implicit formulation of the TSM-ALE-AC system takes the form :

$$\begin{aligned}\left(1+\sum_k C_{(i,k),n}^m\right)\Delta \mathbf{w}_{i,n}^m = \quad & -\Delta\tau_{i,n}^m\,\mathcal{R}_{i,n}^t(\mathbf{w}^m) - \frac{\Delta\tau_{i,n}^m}{2|C_{i,n}|}\sum_k \left(\Delta \mathbf{F}_{o(i,k),n}^E\right)^m \cdot \mathbf{n}_{(i,k),n}|\Gamma_{(i,k),n}| \\ & + \sum_k C_{(i,k),n}^m \Delta \mathbf{w}_{(o(i,k),n}^m - \Delta\tau_{i,n}^m \mathbf{K} \sum_{p=-N}^{N} d_p \Delta \mathbf{w}_{i,n+p}^m \end{aligned} \tag{23}$$

with the scalar coefficients $C_{(i,k),n}^m$ defined by :

$$C_{(i,k),n}^m = \frac{\Delta\tau_{i,n}^m}{|C_{i,n}|}\left(\frac{1}{2}\rho(\mathbf{J}_\perp^E) + \widetilde{\rho(\mathbf{J}_\perp^V)}\right)_{(i,k),n}^m |\Gamma_{(i,k),n}|$$

and $d_0 = 0$ in the spectral time-derivative so that there is no contribution of this term the left-hand-side of (23). Following the strategy adopted to solve the BDF-ALE-AC system, a Point-Jacobi technique is applied to solve (23). However the off-diagonal terms with coefficients d_p introduced in the right-hand-side of (23) lead to a loss of diagonal dominance - this issue was pointed out in [19] [20]. The simple fix adopted in the presented work is derived from [21] : the contribution $\mathbf{K}\sum_{p=-N}^{N}|d_p|$ is simply added to the LHS of the implicit system so as to recover the diagonal dominance property, at the expense of a potential loss of efficiency. In practice, the following PJ-TSM-ALE-AC system yields a satisfactory convergence rate to steady-state :

$$\begin{aligned} & \Delta \mathbf{w}_{i,n}^{(0)} = 0 \\ & \left\{ \begin{array}{l} l = 0, l_{max} - 1 \\ \Delta \mathbf{w}_{i,n}^{(l+1)} = \quad (\mathbf{D}_{i,n}^m)^{-1}\left(-\Delta\tau_{i,n}^m\,\mathcal{R}_{i,n}^t(\mathbf{w}^m) - \frac{\Delta\tau_{i,n}^m}{2|C_{i,n}|}\sum_k \left(\Delta \mathbf{F}_{o(i,k),n}^E\right)^{(l)} \cdot \mathbf{n}_{(i,k),n}|\Gamma_{(i,k),n}| \right. \\ \qquad\qquad \left. + \sum_k C_{(i,k),n}^m \Delta \mathbf{w}_{o(i,k),n}^{(l)} - \Delta\tau_{i,n}^m \mathbf{K} \sum_{p=-N}^{N} d_p \Delta \mathbf{w}_{i,n+p}^{(l)} \right) \end{array} \right. \\ & \mathbf{w}_{i,n}^{m+1} = \mathbf{w}_{i,n}^m + \Delta \mathbf{w}_{i,n}^{(l_{max})} \end{aligned} \tag{24}$$

with the modified diagonal coefficient :

$$D_{i,n}^m = \mathbf{I} + \Delta\tau_{i,n}^m \mathbf{K} \sum_{p=-N}^{N} |d_p| + \sum_k C_{(i,k),n}^m \mathbf{I} \tag{25}$$

3.4 Application

The baseline PH configuration ($\theta_0 = 60°$, $H_0 = 1$ and $f^\star = 0.18$) has been first computed on an unstructured grid containing 32000 cells, with 360 points set on the airfoil surface and a near body resolution tailored to accurately represent the shear-flow regions (see Fig. 1). A reference solution is computed using the BDF approach with 520 times-steps per period; next, the TSM approach is applied with an increasing number of modes until the difference between the reconstructed TSM solution and the reference BDF solution can be considered negligible. As previously demonstrated in [21], using the TSM approach with 17 modes is sufficient to yield a very accurate solution (see Figure 2). As far as computational cost is concerned, the TSM approach offers a substantial reduction (by a factor 4 to 5) with respect to the conventional time-marching approach : the BDF strategy requires about 5 cycles (with 520 physical time-steps per cycle and about 100 dual-time sub-iterations at each physical time-step) to yield an established periodic flow solution while the TSM strategy yields a steady state for the 17 modes after about 3500 iterations (see Fig.3). When the airfoil motion becomes uncertain, the heaving amplitude H_0 is no longer a fixed value but a random variable described by a probability distribution function (pdf). The next Section is devoted to the description of two possible strategies for handling the propagation of this uncertainty through the BDF or TSM unsteady

simulation.

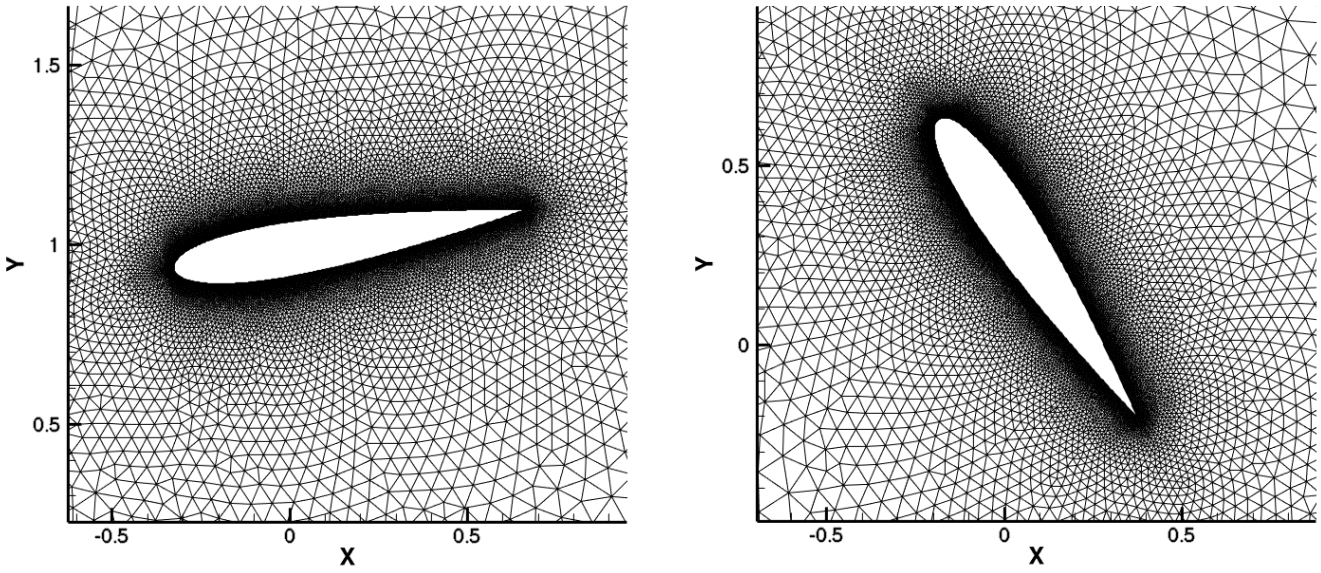

Figure 1: View of the computational grid close to the airfoil surface at two time instances during a period of the flow evolution.

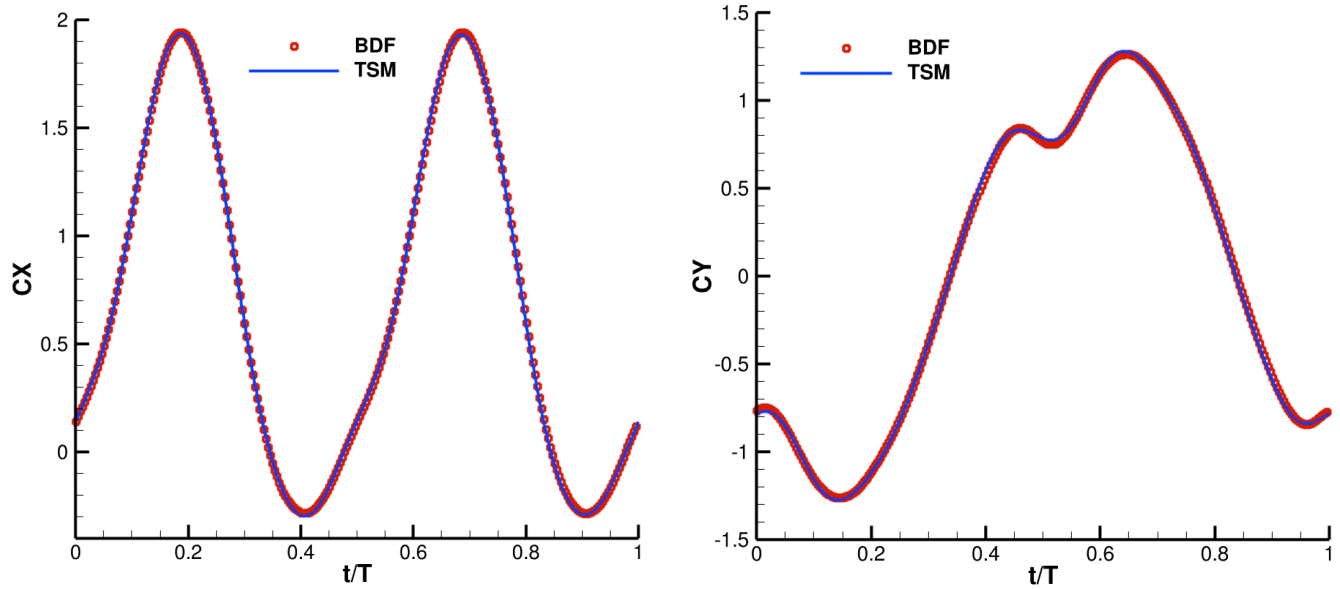

Figure 2: Computed evolutions of C_X and C_Y over a flow period for $\theta_0 = 60°$, $H_0 = 1$ and $f^\star = 0.18$. BDF : 520 time-steps per period (only 1 out of 2 points is plotted). TSM : reconstructed solution using 17 modes.

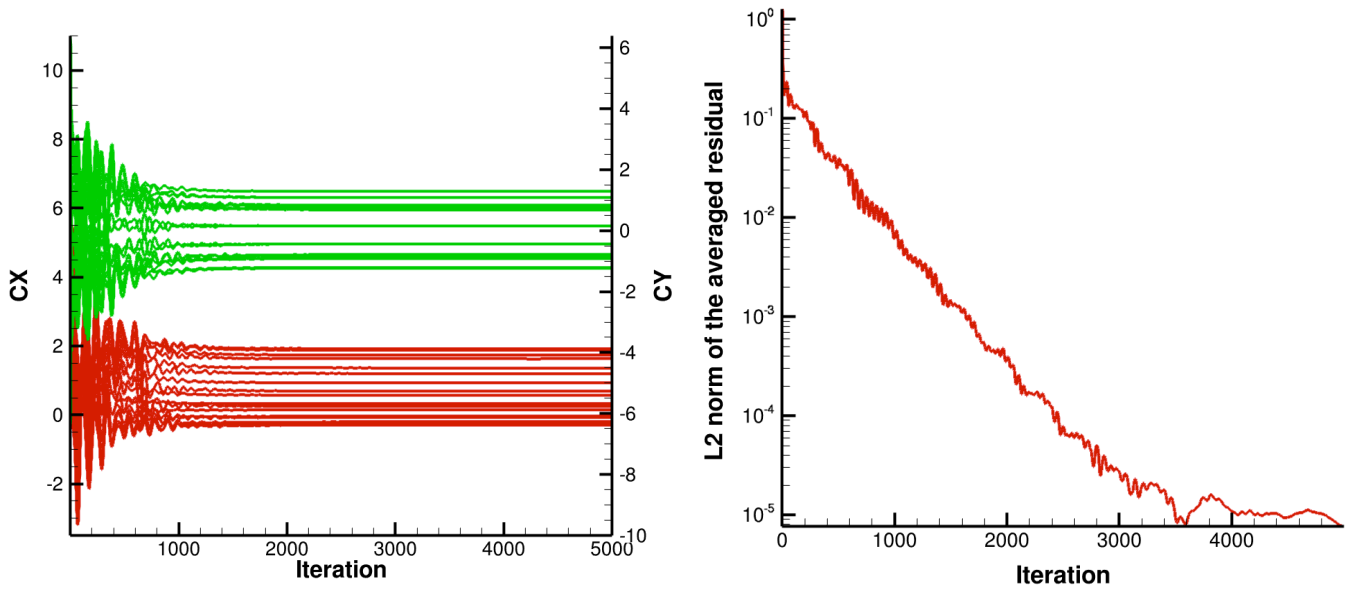

Figure 3: Convergence of the TSM computation (17 modes). Left : evolution of C_X and C_Y to steady values for each mode. Right : evolution to steady-state of the averaged (continuity) residual over the TSM modes .

4 Uncertainty quantification

4.1 Non Intrusive Polynomial Chaos

4.1.1 Principles

Polynomial Chaos (PC) expansions are derived from the original theory of Wiener on spectral representation of stochastic processes using Gaussian random variables. PC expansions have been used for UQ by Ghanem and Spanos [4] and extended by Xiu and Karniadakis [5] to non-Gaussian processes. Any well-behaved process y can be expanded in a convergent series of the form :

$$y(x,t,\xi) = \sum_{\alpha} y_\alpha(x,t)\Psi_\alpha(\xi) \tag{26}$$

where ξ is a set of n_ξ independent random variables $\xi = (\xi_1, \ldots, \xi_{n_\xi})$ and α a multi-index $\alpha = (\alpha_1, \ldots, \alpha_{n_\xi})$. The multivariate function Ψ_α is defined by a product of orthogonal polynomials $\Phi_i^{\alpha_i}(\xi_i)$ in relation to the probability density of the random variable ξ_i, namely $\Psi_\alpha(\xi) = \prod_{i=1}^{n} \Phi_i^{\alpha_i}(\xi_i)$. A one-to-one correspondence exists between the choice of stochastic variable ξ_i and the polynomials $\Phi_i^{\alpha_i}(\xi_i)$ of degree α_i. For instance, if ξ_i is a normal / uniform variable, the corresponding $\Phi_i^{\alpha_i}(\xi_i)$ are Hermite / Legendre polynomials of degree α_i; the degree of Ψ_α is $|\alpha|_1 = \sum_{i=1}^{n_\xi} \alpha_i$. The multivariate polynomial functions Ψ_α are orthogonal with respect to the probability distribution function of the vector ξ of standard independent random variables ξ_i, $i = 1, \ldots, n_\xi$. For practical use, the PC expansion has to be truncated in terms of polynomial degree :

$$y(x,t,\xi) = \sum_{|\alpha|_1 \leq n_o} y_\alpha(x,t)\Psi_\alpha(\xi) \tag{27}$$

The number N_Ψ of multivariate polynomials Ψ_α, that is the dimension of the expansion basis, is related to the stochastic dimension n_ξ and the highest degree n_o of the polynomials by the formula $N_\Psi = (n_\xi + n_o)!/(n_\xi!\, n_o!)$. Several approaches can be used to estimate PC coefficients. The first approach is based on a

Galerkin projection of the model equations : it leads to a set of coupled equations and requires an in-depth adaptation of the deterministic code in order to be applied. Alternative non-intrusive approaches are based on Monte-Carlo simulations or quadrature formulae to evaluate PC coefficients (see for instance [23]). For these non-intrusive approaches, PC coefficients are evaluated from a set of points and weights (ξ_i, ω_i) by formulae of the from :

$$y_\alpha(x,t) = ||\Psi_\alpha||^{-2} \sum_{i=1}^{n} y(x,t,\xi_i)\, \Psi_\alpha(\xi_i)\, \omega_i \tag{28}$$

From the PC expansion (27), it is easy to derive the mean E and variance σ of the random process. If an orthonormal basis is chosen ($||\Psi_\alpha|| = 1\ \forall\alpha$), the following equalities hold :

$$\begin{aligned} E(y(x,t,\xi)) &= y_0(x,t) \\ \sigma(y(x,t,\xi)) &= \sum_\alpha y_\alpha^2(x,t) \end{aligned} \tag{29}$$

4.1.2 Implementation

The practical implementation of NIPC is straightforward and can be decomposed into 3 steps :

- Step 1 : generate, using NISP, the set of quadrature points and weights (ξ_i, ω_i) corresponding to the type of pdf describing the stochastic variable H_0 and to the maximum polynomial order n_o
- Step 2 : compute, using the available CFD solver, the deterministic flows $y(x,t,\xi_i)$ corresponding to the previously generated stochastic DOE for ξ_i
- Step 3 : post-process the quantities of interest using the weights provided by NISP to compute $y_\alpha(x,t)$ from (28) and to estimate the expectation and variance of the quantities of interest from (29).

The CFD solver applied in Step 2 can be either of BDF or of TSM type.

4.2 Semi-intrusive strategy

4.2.1 Principles

The probabilistic solution is numerically described by its conditional expectancies of point values or cell averages and its evaluation is constructed from the deterministic scheme, relying on a tessellation of the random space as in finite volume methods for the space variables. From these conditional expectancies and the geometrical description of the tessellation, a piecewise polynomial approximation in the random variables is computed using a reconstruction method that is standard for high order finite volume space, except that the measure is no longer the standard Lebesgue measure but the probability measure. This reconstruction is then used to formulate a scheme on the numerical approximation of the solution from the deterministic scheme. The proposed approach is said semi-intrusive because, as will be described in the next paragraphs, it requires only a limited amount of modification in an existing deterministic solver to quantify uncertainty on the output state of some quantities of interest when the solver includes uncertain variables.
The domain of variation Ω of the stochastic variable is discretized using in the present case a uniform grid made of n_{prob} cells. Let use denote $\mathbf{w}_{i,j} = E(\mathbf{w}_i|\Omega_j)$ the cell-averaged (over cell C_i of the physical domain) conditional expectancy on cell Ω_j of the random space. In the present study, the $1D$ random space is uniformly discretized so that $\Omega_j = [\omega_{j-\frac{1}{2}}, \omega_{j+\frac{1}{2}}]$ with $\omega_{j\pm\frac{1}{2}} = \omega_j \pm \frac{\Delta\omega}{2}$ with $\Delta\omega = (\omega_{max} - \omega_{min})/n_{prob}$. In order to derive equations of evolution for this conditional expectancy, let us compute the expectancy of the BDF-ALE-AC system (9) - disregarding the iterative dual-time solution for the time being. Taking advantage of the linearity of the physical time-discretization yields :

$$\mathbf{K}\mathcal{T}(\mathbf{w}_{i,j}^{n+1}, \mathbf{w}_{i,j}^{n}, \mathbf{w}_{i,j}^{n-1}) + E(\mathcal{R}_i^{n+1}(\mathbf{w})|\Omega_j) = 0 \tag{30}$$

The remaining key issue is to estimate the conditional expectancy of the residual in terms of the conditional expectancies $\mathbf{w}_{i,j}$. The definition of the residual leads to :

$$\begin{aligned} E(\mathcal{R}_i(\mathbf{w})|\Omega_j) &= E(\mathcal{R}_i^E(\mathbf{w})|\Omega_j) - E(\mathcal{R}_i^V(\mathbf{w})|\Omega_j) \\ &= \frac{1}{|C_i|}\sum_k \left[E(\mathcal{H}_{i,k}^E|\Omega_j) - E(\mathcal{H}_{i,k}^V|\Omega_j)\right]|\Gamma_{i,k}| \end{aligned}$$

The conditional expectancy of the inviscid numerical flux is defined as :

$$E(\mathcal{H}_{i,k}^E|\Omega_j) = \frac{1}{\mu(\Omega_j)}\int_{\Omega_j} \mathcal{H}_{i,k}^E(\omega)\,\mu(\omega)d\omega \tag{31}$$

where the stochastic inviscid flux $\mathcal{H}_{i,k}^E(\omega)$ is computed from the definition (7) applied with a polynomial approximation $\mathbf{P}_{i,j}$ of the stochastic solution in cell Ω_j :

$$\mathcal{H}_{i,k}^E(\omega) = \mathcal{H}^E(\mathbf{P}_{i,j}(\omega), \nabla\mathbf{P}_{i,j}(\omega); \mathbf{P}_{o(i,k),j}(\omega), \nabla\mathbf{P}_{o(i,k),j}(\omega))$$

A possible choice for $\mathbf{P}_{i,j}$ will be detailed below; at this stage, it is sufficient to keep in mind $\mathbf{P}_{i,j}$ will be typically a linear combination of the conditional expectancies $\mathbf{w}_{i-1,j}$, $\mathbf{w}_{i,j}$ and $\mathbf{w}_{i+1,j}$. A standard third-order Gaussian quadrature is used to numerically estimate the integral appearing in (31). Denoting ω_{j_1} and ω_{j_2} the two quadrature points in Ω_j and p_{j_1}, p_{j_2} their respective quadrature weights, the conditional expectancy of the inviscid numerical flux is evaluated as :

$$E(\mathcal{H}_{i,k}^E|C_j) = \beta_{j_1}\mathcal{H}^E(\mathbf{P}_{i,j}(\omega_{j_1}); \mathbf{P}_{o(i,k),j}(\omega_{j_1})) + \beta_{j_2}\mathcal{H}^E(\mathbf{P}_{i,j}(\omega_{j_2}); \mathbf{P}_{o(i,k),j}(\omega_{j_2})) \tag{32}$$

where the dependence of the numerical flux formula on the gradients $\nabla\mathbf{P}$ has been omitted and with weights β_{j_1}, β_{j_2} defined as $\beta_{j_{(1,2)}} = \dfrac{\mu(\omega_{j_{(1,2)}})p_{j_{(1,2)}}}{\mu(\Omega_j)}$. The conditional expectancy of the viscous numerical flux over cell Ω_j is similarly computed as :

$$\begin{aligned} E(\mathcal{H}_{i,k}^V|\Omega_j) &= \frac{1}{\mu(\Omega_j)}\int_{\Omega_j} \mathcal{H}_{i,k}^V(\omega)\,\mu(\omega)d\omega \\ &\approx \frac{1}{\mu(\Omega_j)}\int_{\Omega_j} \mathcal{H}^V(\nabla\mathbf{P}_{N_{i,k}^1,j}(\omega); \nabla\mathbf{P}_{N_{i,k}^2,j}(\omega))\,\mu(\omega)d\omega \\ &\approx \beta_{j_1}\mathcal{H}^V(\nabla\mathbf{P}_{N_{i,k}^1,j}(\omega_{j_1}); \nabla\mathbf{P}_{N_{i,k}^2,j}(\omega_{j_1})) + \beta_{j_2}\mathcal{H}^V(\nabla\mathbf{P}_{N_{i,k}^1,j}(\omega_{j_2}); \nabla\mathbf{P}_{N_{i,k}^2,j}(\omega_{j_2})) \end{aligned} \tag{33}$$

Inserting (32) and (33) into (30) yields :

$$\left\{ \begin{array}{l} \mathbf{K}\mathcal{T}(\mathbf{w}_{i,j}^{n+1}, \mathbf{w}_{i,j}^{n}, \mathbf{w}_{i,j}^{n-1}) + \dfrac{1}{|C_i|}\displaystyle\sum_k \left[\beta_{j_1}\mathcal{H}(\mathbf{P}_{\cdot,j}^{n+1}(\omega_{j_1})) + \beta_{j_2}\mathcal{H}(\mathbf{P}_{\cdot,j}^{n+1}(\omega_{j_2}))\right]|\Gamma_{i,k}| = 0 \\ \\ \text{with the numerical flux } \mathcal{H}(\mathbf{P}_{\cdot,j}(\omega)) \text{ computed as} \\ \\ \mathcal{H}(\mathbf{P}_{\cdot,j}^{n+1}(\omega)) = \mathcal{H}^E(\mathbf{P}_{i,j}^{n+1}(\omega); \mathbf{P}_{o(i,k),j}^{n+1}(\omega)) - \mathcal{H}^V(\nabla\mathbf{P}_{N_{i,k}^1,j}^{n+1}(\omega); \nabla\mathbf{P}_{N_{i,k}^2,j}^{n+1}(\omega)) \end{array} \right. \tag{34}$$

For (34) to define the time-evolution of the expectancies $\mathbf{w}_{i,j}$ it remains to specify the expression of the polynomial reconstruction $\mathbf{P}_{\cdot,j}^{n+1}(\omega)$ for the stochastic solution at point $\cdot$ of the physical domain (where $\cdot$ can be a cell center, for instance i or $o(i,k)$, or a cell node, for instance $N_{i,k}^1$ or $N_{i,k}^2$). To achieve second-order accuracy, the following quadratic polynomial reconstruction is used in cell Ω_j centered on ω_j :

$$\mathbf{P}_{i,j} = \mathbf{a} + \mathbf{b}\,(\omega - \omega_j) + \mathbf{c}\,(\omega - \omega_j)^2$$

The coefficients **a**, **b** and **c** are determined by requiring $E(\mathbf{P}_{i,l}|\Omega_l) = E(\mathbf{w}_{i,l}|\Omega_l) = \mathbf{w}_{i,l}$ for $l = j-1, j, j+1$. Since the same reconstruction is applied to each component of $\mathbf{P}_{i,j}$, the coefficients a, b and c can be considered as scalars and are such that :

$$\underbrace{\begin{pmatrix} 1 & E(\omega-\omega_j|\Omega_{j-1}) & E((\omega-\omega_j)^2|\Omega_{j-1}) \\ 1 & E(\omega-\omega_j|\Omega_j) & E((\omega-\omega_j)^2|\Omega_j) \\ 1 & E(\omega-\omega_j|\Omega_{j+1}) & E((\omega-\omega_j)^2|\Omega_{j+1}) \end{pmatrix}}_{=\mathbf{M}_j} \cdot \begin{pmatrix} a \\ b \\ c \end{pmatrix} = \begin{pmatrix} \mathbf{w}_{i,j-1} \\ \mathbf{w}_{i,j} \\ \mathbf{w}_{i,j+1} \end{pmatrix}$$

For a given pdf and a fixed discretization of the stochastic space Ω, the matrix $\mathbf{M}$ can be computed and inverted once for all the start of the calculation. Let us denote :

$$\mathbf{M}_j^{-1} = \begin{pmatrix} a_j^- & a_j^0 & a_j^+ \\ b_j^- & b_j^0 & b_j^+ \\ c_j^- & c_j^0 & c_j^+ \end{pmatrix}$$

An immediate calculation yields the following expression for the polynomial reconstruction :

$$\mathbf{P}_{i,j}^{n+1}(\omega) = \alpha_j^-(\omega)\,\mathbf{w}_{i,j-1}^{n+1} + \alpha_j^0(\omega)\,\mathbf{w}_{i,j}^{n+1} + \alpha_j^+(\omega)\,\mathbf{w}_{i,j+1} \tag{35}$$

with

$$\begin{cases} \alpha_j^-(\omega) = a_j^- + b_j^-(\omega-\omega_j) + c_j^-(\omega-\omega_j)^2 \\ \alpha_j^0(\omega) = a_j^0 + b_j^0(\omega-\omega_j) + c_j^0(\omega-\omega_j)^2 \\ \alpha_j^+(\omega) = a_j^+ + b_j^+(\omega-\omega_j) + c_j^+(\omega-\omega_j)^2 \end{cases} \tag{36}$$

This same linear combination can be applied on the cell-center gradients $\nabla\mathbf{w}_{i,j-1}$, $\nabla\mathbf{w}_{i,j}$, $\nabla\mathbf{w}_{i,j+1}$ to compute the quantities $\nabla\mathbf{P}_{i,j}$ necessary to the second-order evaluation of the inviscid numerical flux and also on the node gradients $\nabla\mathbf{w}_{N,j-1}$, $\nabla\mathbf{w}_{N,j}$, $\nabla\mathbf{w}_{N,j+1}$ to compute the quantities $\nabla\mathbf{P}_{N^1_{(i,k),j}}$, $\nabla\mathbf{P}_{N^2_{(i,k),j}}$ used in the viscous flux evaluation.

4.2.2 Implementation of the SI-BDF-ALE-AC approach

The final formulation of the SI-BDF-ALE-AC system is obtained from the following steps :

$$\begin{cases} \bullet \text{ Polynomial reconstruction of } \mathbf{w}_{\cdot,j},\ \nabla\mathbf{w}_{\cdot,j} \text{ at cell centers and nodes} \\ \quad \text{applying (35) with } \mathbf{w}_{i,j},\ \mathbf{w}_{N,j} \text{ and } \nabla\mathbf{w}_{i,j},\ \nabla\mathbf{w}_{N,j} \\ \quad \Rightarrow \quad \mathbf{P}_{i,j}, \mathbf{P}_{N,j}, \nabla\mathbf{P}_{i,j}, \nabla\mathbf{P}_{N,j} \\ \\ \bullet \text{ Inviscid numerical flux :} \\ \mathcal{H}^E_{(i,k),j} = \beta_{j_1}\mathcal{H}^E(\mathbf{P}_{i,j}^{n+1}(\omega_{j_1}); \mathbf{P}^{n+1}_{o(i,k),j}(\omega_{j_1})) + \beta_{j_2}\mathcal{H}^E(\mathbf{P}_{i,j}^{n+1}(\omega_{j_2}); \mathbf{P}^{n+1}_{o(i,k),j}(\omega_{j_2})) \\ \\ \bullet \text{ Viscous numerical flux :} \\ \mathcal{H}^V_{(i,k),j} = \beta_{j_1}\mathcal{H}^V(\nabla\mathbf{P}_{N^1_{i,k},j}(\omega_{j_1}); \nabla\mathbf{P}_{N^2_{i,k},j}(\omega_{j_1})) + \beta_{j_2}\mathcal{H}^V(\nabla\mathbf{P}_{N^1_{i,k},j}(\omega_{j_2}); \nabla\mathbf{P}_{N^2_{i,k},j}(\omega_{j_2})) \\ \\ \bullet \text{ Inviscid, viscous and total residual :} \\ \mathcal{R}^E_{i,j} = \dfrac{1}{|C_i|}\displaystyle\sum_k \mathcal{H}^E_{(i,k),j}|\Gamma_{i,k}|, \quad \mathcal{R}^V_{i,j} = \dfrac{1}{|C_i|}\displaystyle\sum_k \mathcal{H}^V_{(i,k),j}|\Gamma_{i,k}|, \quad \mathcal{R}_{i,j} = \mathcal{R}^E_{i,j} - \mathcal{R}^V_{i,j} \\ \\ \bullet \text{ SI-BDF-ALE-AC system :} \\ \mathbf{K}\mathcal{T}(\mathbf{w}_{i,j}^{n+1}, \mathbf{w}_{i,j}^{n}, \mathbf{w}_{i,j}^{n-1}) + \mathcal{R}_{i,j}^{n+1} = \mathcal{R}_{i,j}^{t}(\mathbf{w}^{n+1}) = 0 \end{cases} \tag{37}$$

The semi-intrusive nature of the proposed UQ strategy appears now clearly when comparing the above formulation of the SI-BDF-ALE-AC system with the deterministic CFD solver described in Section 3 : the very structure of the solution algorithm remains basically unchanged, with the stochastic solution $\mathbf{w}_{i,j}$ or its polynomial reconstruction $\mathbf{P}_{i,j}$ replacing the purely deterministic physical state $\mathbf{w}_i$ and a two-point

quadrature in the stochastic space which leads to a double evaluation of the (unchanged) inviscid and viscous numerical flux formulae on each face of the physical domain. In order to solve the implicit system coupling the unknown expectancies $\mathbf{w}_{\{i\},j-1}$, $\mathbf{w}_{\{i\},j}$, $\mathbf{w}_{\{i\},j+1}$, where i denotes the whole set of space grid points involved in the space discretization of the system, a sub-iterative strategy or dual-time strategy is applied. This strategy can be defined by following the steps described in section 3.2 for the deterministic case. The states $\mathbf{w}_{i,j}^{n+1}$ are found as the steady solution of the implicit dual-time marching problem :

$$\Delta \mathbf{w}_{i,j}^{n,m} = -\Delta \tau_{i,j}^{n,m} \mathcal{R}_{i,j}^{t}(\mathbf{w}^{n,m+1})$$

where $\Delta \mathbf{w}_{i,j}^{n,m} = \mathbf{w}_{i,j}^{n,m+1} - \mathbf{w}_{i,j}^{n,m}$. The total residual is approximately expanded as :

$$\mathcal{R}_{i,j}^{t}(\mathbf{w}^{n,m+1}) \approx \mathcal{R}_{i,j}^{t}(\mathbf{w}^{n,m}) + \frac{3}{2}\frac{\mathbf{K}}{\Delta t}\Delta \mathbf{w}_{i,j}^{n,m} + \mathcal{I}(\Delta \mathbf{w}^{n,m})$$

with $\mathcal{I}(\Delta \mathbf{w}^{n,m})$ a simplified estimate of $\left(\frac{d\mathcal{R}_i}{d\mathbf{P}}\right)^{n,m} \Delta \mathbf{P}^{n,m}$. Two main options exist to deal with this contribution to the implicit stage : either to expand the term using the second-order polynomial approximation (35) for $\Delta \mathbf{P}$ or to keep a simplified first-order approximation ($\Delta \mathbf{P} = \Delta \mathbf{w}$). The former option leads to a more consistent implicit / explicit treatment, which should translate into a more efficient convergence to a steady-state, balancing the extra-cost associated with the added terms $\Delta \mathbf{w}_{\{i\},j-1}$, $\Delta \mathbf{w}_{\{i\},j+1}$. At this preliminary stage of the SI-BDF-ALE-AC implementation, a first-order implicit treatment will be favored because of the very few modifications it required in the baseline deterministic implicit treatment. Indeed, the final form of the PJ-SI-BDF-ALE-AC system reads :

$$\begin{array}{l} \Delta \mathbf{w}_{i,j}^{(0)} = 0 \\ \left\{ \begin{array}{l} l = 0, l_{max} - 1 \\ \Delta \mathbf{w}_{i,j}^{(l+1)} = (\mathbf{D}_{i,j}^{n,m})^{-1} \left(-\Delta \tau_{i,j}^{n,m} \mathcal{R}_{i,j}^{t}(\mathbf{w}^{n,m}) - \dfrac{\Delta \tau_{i,j}^{n,m}}{2|C_i|} \displaystyle\sum_k \left(\Delta \mathbf{F}_{o(i,k),j}^{E} \right)^{(l)} \cdot \mathbf{n}_{(i,k),j} |\Gamma_{i,k}| + \sum_k C_{i,k,j}^{n,m} \Delta \mathbf{w}_{o(i,k),j}^{(l)} \right) \end{array} \right. \\ \mathbf{w}_{i,j}^{n,m+1} = \mathbf{w}_{i,j}^{n,m} + \Delta \mathbf{w}_{i,j}^{(l_{max})} \end{array} \tag{38}$$

with the matrix $\mathbf{D}_i^{n,m}$ and scalars $C_{i,k}^{n,m}$ defined as :

$$\mathbf{D}_{i,j}^{n,m} = \left(\mathbf{I} + \frac{3}{2}\frac{\Delta \tau_{i,j}^{n,m}}{\Delta t}\mathbf{K} + \sum_k C_{(i,k),j}^{n,m} \mathbf{I} \right) \quad , \quad C_{(i,k),j}^{n,m} = \frac{\Delta \tau_{i,j}^{n,m} |\Gamma_{i,k}|}{|C_i|} \left(\frac{1}{2}\rho(\mathbf{J}_{\perp}^{E}) + \rho(\widetilde{\mathbf{J}_{\perp}^{V}}) \right)_{(i,k),j}^{n,m} \tag{39}$$

The above system is identical to the system (10)-(11) solved in the deterministic solver, with the conditional expectation $\mathbf{w}_{i,j}$ replacing the deterministic solution $\mathbf{w}_i$.

4.2.3 Implementation of the SI-TSM-ALE-AC approach

Computing the conditional expectancy of the TSM-ALE-AC system (20) and taking advantage of the linearity of the spectral time-discretization yields :

$$\mathbf{K} D_t(\mathbf{w}_{i,n,j}) + E(\mathcal{R}_{i,n}(\mathbf{w}, \mathbf{x}, \mathbf{s}) | \Omega_j) = 0, \qquad 0 \leq n < 2N + 1 \tag{40}$$

where $\mathbf{w}_{i,n,j} = E(\mathbf{w}_{i,n} | \Omega_j)$ is the conditional expectation of the n^{th} TSM mode at cell-center i over the cell Ω_j in the stochastic space and the residual $\mathcal{R}_{i,n}$ is computed in each grid cell i at each time instance t_n over the period T, corresponding to the n^{th} TSM mode. The key ingredients of the SI approach applied to the TSM-ALE-AC system are similar to the ones previously described for the BDF-ALE-AC system : the conditional expectation of the residual over cell Ω_j is obtained from the conditional expectation of the inviscid and viscous numerical fluxes; the flux conditional expectations are computed using a second-order quadrature formula over Ω_j and a second-order polynomial reconstruction of the stochastic solution in cell

Ω_j. The main steps of the SI-TSM-ALE-AC treatment can be summarized as follows :

$$\left\{\begin{array}{l}
\bullet \text{ Polynomial reconstruction of } \mathbf{w}_{i/N,n,j},\ \nabla\mathbf{w}_{i/N,n,j} \text{ at cell centers and nodes for the } n^{th} \text{ TSM mode} \\
\quad \text{applying (35) with } \mathbf{w}_{i,n,j},\ \mathbf{w}_{N,n,j} \text{ and } \nabla\mathbf{w}_{i,n,j},\ \nabla\mathbf{w}_{N,n,j} \\
\quad \Rightarrow \quad \mathbf{P}_{i,n,j}, \mathbf{P}_{N,n,j}, \nabla\mathbf{P}_{i,n,j}, \nabla\mathbf{P}_{N,n,j} \\
\\
\bullet \text{ Inviscid numerical flux :} \\
\mathcal{H}^E_{(i,k),n,j} = \beta_{j_1}\mathcal{H}^E(\mathbf{P}_{i,n,j}(\omega_{j_1}); \mathbf{P}_{o(i,k),n,j}(\omega_{j_1})) + \beta_{j_2}\mathcal{H}^E(\mathbf{P}_{i,n,j}(\omega_{j_2}); \mathbf{P}_{o(i,k),n,j}(\omega_{j_2})) \\
\\
\bullet \text{ Viscous numerical flux :} \\
\mathcal{H}^V_{(i,k),n,j} = \beta_{j_1}\mathcal{H}^V(\nabla\mathbf{P}_{N^1_{i,k},n,j}(\omega_{j_1}); \nabla\mathbf{P}_{N^2_{i,k},n,j}(\omega_{j_1})) + \beta_{j_2}\mathcal{H}^V(\nabla\mathbf{P}_{N^1_{i,k},n,j}(\omega_{j_2}); \nabla\mathbf{P}_{N^2_{i,k},n,j}(\omega_{j_2})) \\
\\
\bullet \text{ Inviscid, viscous and total residual :} \\
\quad \mathcal{R}^E_{i,n,j} = \dfrac{1}{|C_i|}\displaystyle\sum_k \mathcal{H}^E_{(i,k),n,j}|\Gamma_{i,k}|, \quad \mathcal{R}^V_{i,n,j} = \dfrac{1}{|C_i|}\displaystyle\sum_k \mathcal{H}^V_{(i,k),n,j}|\Gamma_{i,k}|, \quad \mathcal{R}_{i,n,j} = \mathcal{R}^E_{i,n,j} - \mathcal{R}^V_{i,n,j} \\
\\
\bullet \text{ SI-TSM-ALE-AC system :} \\
\mathbf{K}D_t(\mathbf{w}_{i,n,j}) + \mathcal{R}_{i,n,j}(\mathbf{w}) = \mathcal{R}^t_{i,n,j}(\mathbf{w}) = 0
\end{array}\right. \tag{41}$$

Following the line of idea previously developed in the deterministic case, the SI-TSM-ALE-ACE system is solved thanks to a fictitious or dual-time strategy, looking iteratively on m for the steady solution of :

$$\frac{\mathbf{w}^{m+1}_{i,n,j} - \mathbf{w}^m_{i,n,j}}{\Delta\tau^m_{i,n,j}} + \mathcal{R}^t_{i,n,j}(\mathbf{w}^m) = 0$$

Global efficiency is achieved by making this relationship implicit with respect to the dual time, *i.e.* computing $\mathcal{R}^t_{i,n,j}(\mathbf{w}^{m+1})$ instead of $\mathcal{R}^t_{i,n,j}(\mathbf{w}^m)$. When expanding $\mathcal{R}^t_{i,n,j}(\mathbf{w}^{m+1})$ around subiteration m to derive the implicit stage of the final SI-TSM-ALE-AC system the two options previously encountered in the derivation of the Si-BFD-ALE-AC system appear again : the second-order approximation of the solution in the stochastic space can be included in the implicit stage so as to make it intrinsically more efficient or a simplified first-order implicit stage can be retained, which is potentially less efficient to reach a steady-state but more immediate to implement. The choice made at this stage of development favors the ease of implementation so that the latter option is retained. The PJ-SI-TSM-ALE-AC system reads :

$$\begin{array}{l}
\Delta\mathbf{w}^{(0)}_{i,n,j} = 0 \\
\left\{\begin{array}{l}
l = 0, l_{max} - 1 \\
\Delta\mathbf{w}^{(l+1)}_{i,n,j} = \quad (\mathbf{D}^m_{i,n,j})^{-1}\left(-\Delta\tau^m_{i,n,j}\,\mathcal{R}^t_{i,n,j}(\mathbf{w}^m) - \frac{\Delta\tau^m_{i,n,j}}{2|C_{i,n}|}\displaystyle\sum_k \left(\Delta\mathbf{F}^E_{o(i,k),n,j}\right)^{(l)} \cdot \mathbf{n}_{(i,k),n,j}|\Gamma_{(i,k),n}|\right. \\
\qquad\qquad\qquad\qquad \left. + \displaystyle\sum_k C^m_{(i,k),n,j}\Delta\mathbf{w}^{(l)}_{o(i,k),n,j} - \Delta\tau^m_{i,n,j}\mathbf{K}\displaystyle\sum_{p=-N}^{N} d_p\Delta\mathbf{w}^{(l)}_{i,n+p,j}\right)
\end{array}\right. \\
\mathbf{w}^{m+1}_{i,n,j} = \mathbf{w}^m_{i,n,j} + \Delta\mathbf{w}^{(l_{max})}_{i,n,j}
\end{array} \tag{42}$$

with the coefficients :

$$D^m_{i,n,j} = \mathbf{I} + \Delta\tau^m_{i,n,j}\mathbf{K}\textstyle\sum_{p=-N}^{N}|d_p| + \sum_k C^m_{(i,k),n,j}\mathbf{I} \quad , \quad C^m_{(i,k),n,j} = \dfrac{\Delta\tau^m_{i,n,j}}{|C_{i,n}|}\left(\dfrac{1}{2}\rho(\mathbf{J}^E_\perp) + \widetilde{\rho(\mathbf{J}^V_\perp)}\right)^m_{(i,k),n,j}|\Gamma_{(i,k),n}| \tag{43}$$

When the conditional expectancy $\mathbf{w}_{i,n,j}$ over cell Ω_j of the random space is available for each grid cell i and each TSM mode n, the mean $\overline{w}_{i,n}$ and variance $\sigma(\mathbf{w})_{i,n}$ are computed by means of the following definitions :

$$\overline{w}_{i,n} = \sum_j \mathbf{w}_{i,n,j} \quad , \quad \sigma(\mathbf{w})_{i,n} = \sum_j \int_{\Omega_j} (\overline{w}_{i,n} - \mathbf{w}_{i,n,j})^2 d\mu \tag{44}$$

4.3 Application

The PH problem is now computed with H_0 defined as a stochastic variable; more precisely, the H_0 parameter is assumed to follow a uniform pdf with minimum and maximum values respectively equal to 0.95 and 1.05. The NIPC approach is applied with a maximum polynomial degree equal to 4; using NISP, the 5 points $(H_0)_i$ needed to compute the PC coefficients are obtained. The deterministic computations to be performed for the specific values $(H_0)_i$ in the interval $[0.95, 1.05]$ make use either of the CFD BDF solver or of the CFD TSM solver. Since the greater efficiency of the TSM approach was established in the deterministic case, the TSM solver is used to compute this set of deterministic solutions and 17 TSM modes are used since accurate results were obtained with this choice for $H_0 = 1$ in the deterministic case. The resulting reconstructed evolutions of C_X and C_Y over a flow period are displayed in Figure 4. Each of the 5 computations yields a convergence history to steady-state very similar to the one displayed in Figure 3. Gathering the 17 steady values of $(C_X)_n$ and $(C_Y)_n$ for the 17 TSM modes, the time-evolution of C_X and C_Y can be reconstructed over a flow period for all 5 deterministic runs (see Figure 4). The mean value and variance of C_X and C_Y are readily obtained by post-processing these curves using the weights provided by NISP.
Alternatively the SI-TSM approach can be applied, using $n_{prob} = 5$ cells in order to perform a comparison with the previous NIPC-TSM approach for an *a priori* comparable overall cost. In practice, the NIPC-TSM is naturally parallelizable since the computations corresponding to the set of $(H_0)_i$ values can be executed independently. The SI-TSM approach can also exploit some level of parallelism but in a less straightforward way since the conditional expectations $\mathbf{w}_{i,n,j}$ are coupled by (41). Figure 5 displays the evolution of $(\overline{C_X})_n$, $\sigma(C_X)_n$ and $(\overline{C_Y})_n$, $\sigma(C_Y)_n$ for the 17 TSM modes used in the computation. The mean evolution $\overline{C_X}(t)$ and $\overline{C_Y}(t)$ along with the envelope curves $\overline{C_X}(t) \pm stdev(C_X)(t)$, $\overline{C_Y}(t) \pm stdev(C_Y)(t)$ can be reconstructed from the moments of the TSM modes and compared with the same curves as derived from the NIPC-TSM approach.
The curves plotted in Figure 6 show a good agreement overall between the NICP-TSM and SI-TSM predictions both for C_X and C_Y or more precisely their respective first moments $\overline{C_X}$, $\sigma(C_X)$ and $\overline{C_Y}$, $\sigma(C_Y)$. A close-up on the minimum and maximum levels reached by these curves (in Figure 7 for $\overline{C_X}$, $\overline{C_X} \pm \sqrt{\sigma(C_X)}$ and Figure 8 for $\overline{C_Y}$, $\overline{C_Y} \pm \sqrt{\sigma(C_Y)}$) allow to analyze more finely the difference between the NIPC and the SI prediction. This difference remains systematically low for the C_X curve with superimposed mean curves and a slight underprediction of the variance by the SI approach with respect to NIPC. The same conclusions hold for the C_Y curve with a more pronounced difference in the computed variance close to $t/T = 0$ and $t/T = 0.5$: close to $t/T = 0$ the variance computed using SI-TSM is strongly under predicted with respect to the variance given by NIPC-TSM; reversely, close to $t/T = 0.5$, the NIPC-TSM predicts a lower variance than SI-TSM.
The SI-TSM approach can also be used to compute the mean pressure coefficient and its local variance at any time instance within the flow period as exemplified in Figure 9.

5 Conclusions and perspectives

The first coupling between the incompressible TSM solver developed in [21] and the semi-intrusive UQ method proposed in [12] yields promising results when applied to the prediction of the aerodynamic coefficients for an oscillating airfoil submitted to an uncertain motion. A one-shot calculation allows to obtain the expectations over each cell Ω_j of the stochastic space, $\mathbf{w}_{i,n,j}$, at each grid point i and for each TSM time instance t_n within the period. Using these conditional expectations, it is possible to compute the first moments of any quantity of interest. The comparison performed with the well-established non-intrusive polynomial chaos approach available in the NISP library provides a first qualitative validation of the SI implementation for the simple case of a single uncertain parameter with uniform pdf but several paths need to be explored. A more thorough assessment of the accuracy and efficiency properties of the SI approach with respect to the NIPC strategy is required. In particular, the NIPC-TSM and SI-TSM solutions must be compared when simultaneously increasing n_o and n_{prob} in order to check the grid-convergence property of the SI-TSM strategy. Moreover, simulations using SI-TSM with an arbitrary (for instance discontinuous) pdf will be undertaken to provide a further demonstration of the method's flexibility. When solving the SI-TSM-ALE-AC system, the efficiency of the approach is also likely to be improved through the use of a less simplified implicit stage, taking into account the second-order reconstruction in the stochastic space.

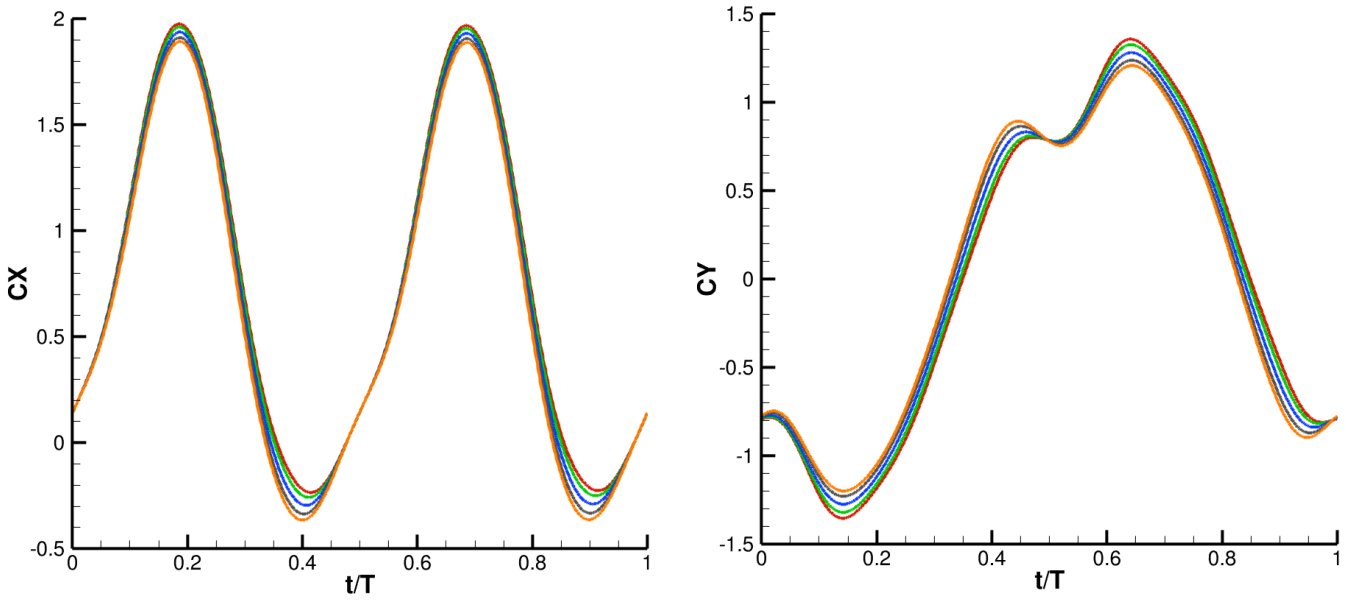

Figure 4: Reconstructed evolution of C_X (left) and C_Y (right) over a flow period, computed with 17 TSM modes for the 5 values of H_0 defining the stochastic DOE (associated with the uniform pdf for H_0 and $n_o = 4$).

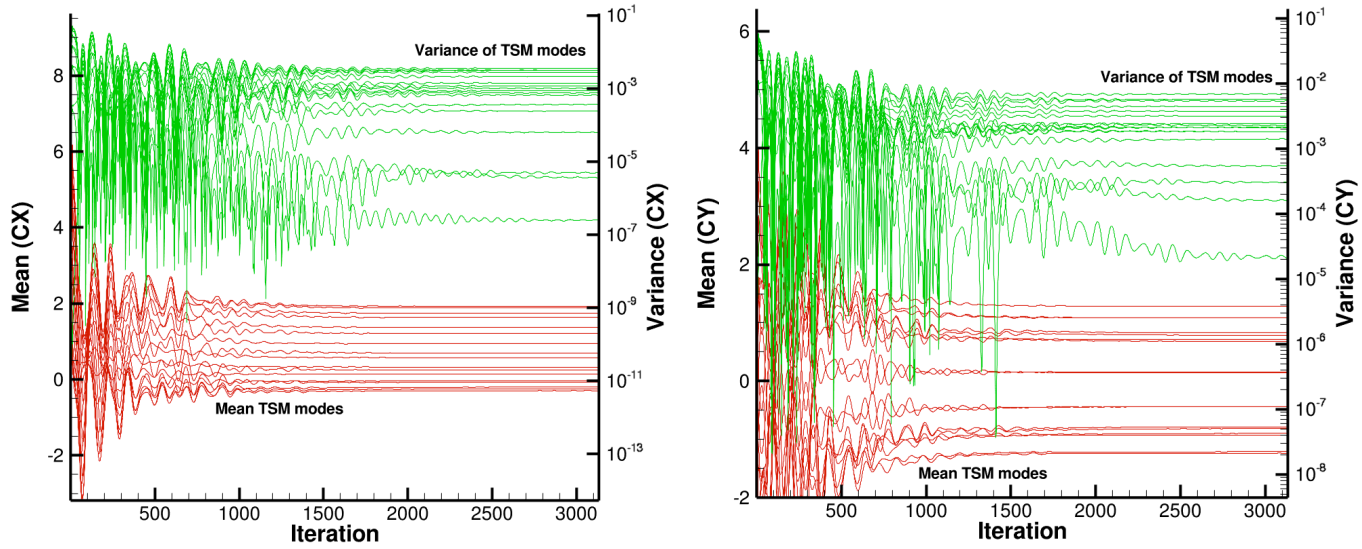

Figure 5: Convergence to steady-state of the SI-TSM computation with $n_{prob} = 5$ and 17 TSM modes. Evolution of $(\overline{C_X})_n$, $\sigma(C_X)_n$ (left) and $(\overline{C_Y})_n$, $\sigma(C_Y)_n$ (right) to steady values for each mode.

References

[1] T. Kinsey, G. Dumas. Parametric Study of an Oscillating Airfoil in a Power-Extraction Regime. *AIAA Journal*, 46:1318-1330, 2008.

[2] H.N. Najm. Uncertainty quantification and polynomial chaos techniques in computational fluid dynamics. *Annu. Rev. Fluid Mech.*, 41:35-52, 2009.

[3] D. Xiu. Fast numerical methods for stochastic computations: a review. *Communications in Computational Physics*, 5(2):242-272, 2009.

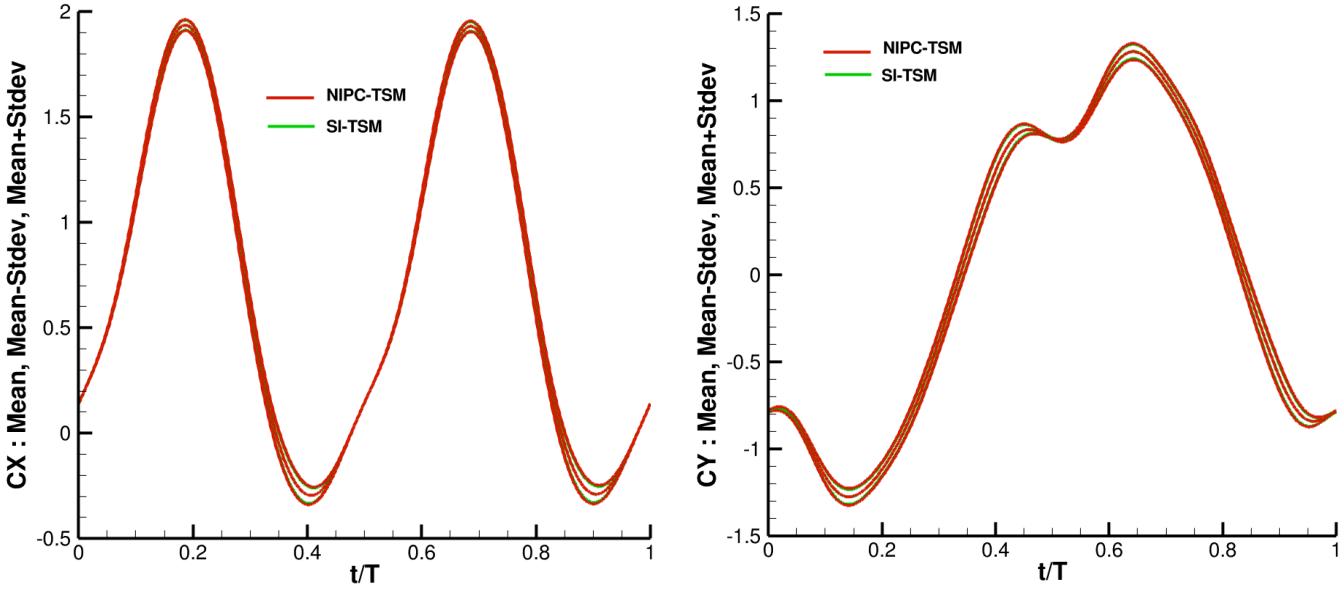

Figure 6: Time evolution of $\overline{C_X}(t)$, $\overline{C_X}(t) \pm \sqrt{\sigma(C_X)(t)}$ (left) and $\overline{C_Y}(t)$, $\overline{C_Y}(t) \pm \sqrt{\sigma(C_Y)(t)}$ (right) over a flow period, computed with NIPC-TSM ($n_o = 4$, $n_{TSM} = 17$) and SI-TSM ($n_{prob} = 5$, $n_{TSM} = 17$).

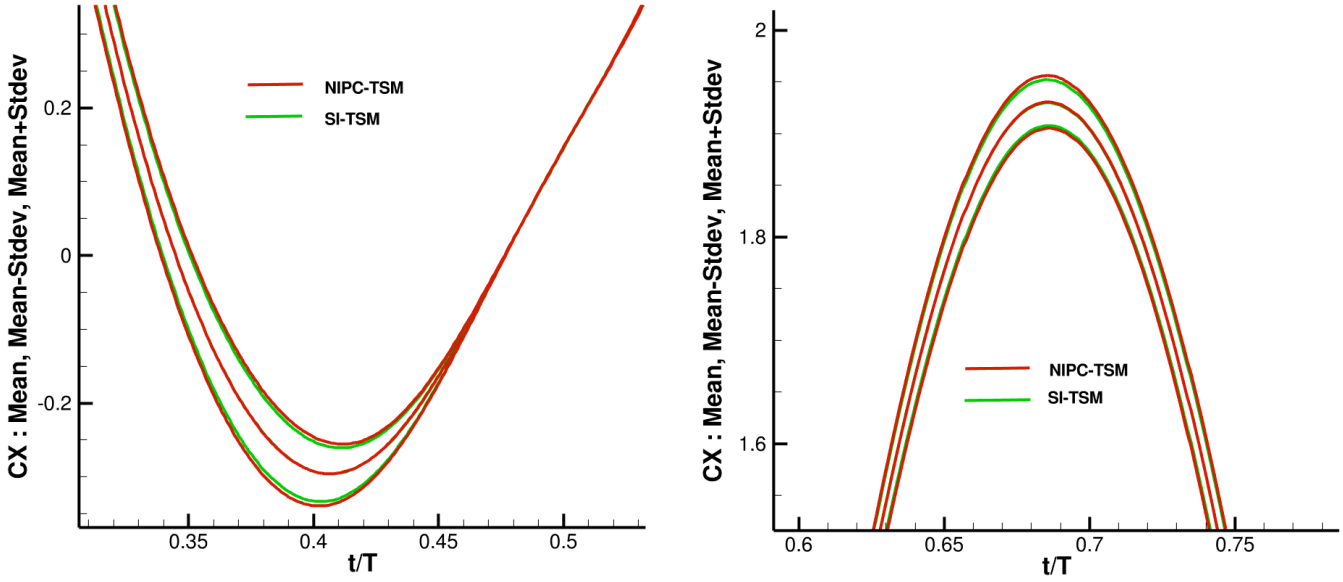

Figure 7: Time evolution of $\overline{C_X}(t)$, $\overline{C_X}(t) \pm \sqrt{\sigma(C_X)(t)}$ over a flow period, computed with NIPC-TSM and SI-TSM. Detailed comparison around minimum (left) and maximum (right) levels.

[4] R.G. Ghanem, S.D. Spanos. *Stochastic Finite Elements : a Spectral Approach*. Springer Verlag, 1991.

[5] D. Xiu, G.E. Karniadakis. The Wiener-Askey polynomial chaos for stochastic differential equations. *SIAM Journal on Scientific Computing*, 24(2):619-644, 2002.

[6] I. Babuska, R. Tempone, G.E. Zouraris. Galerkin finite elements approximation of stochastic elliptic partial differential equations. *SIAM Journal on Numerical Analysis*, 42(2):800-825, 2004.

[7] P.G. Constantine, D.F. Gleich, G. Iaccarino. Spectral methods for parameterized matrix equations. *SIAM Journal on Matrix Analysis and Applications*, 31(5):2681-2699, 2010.

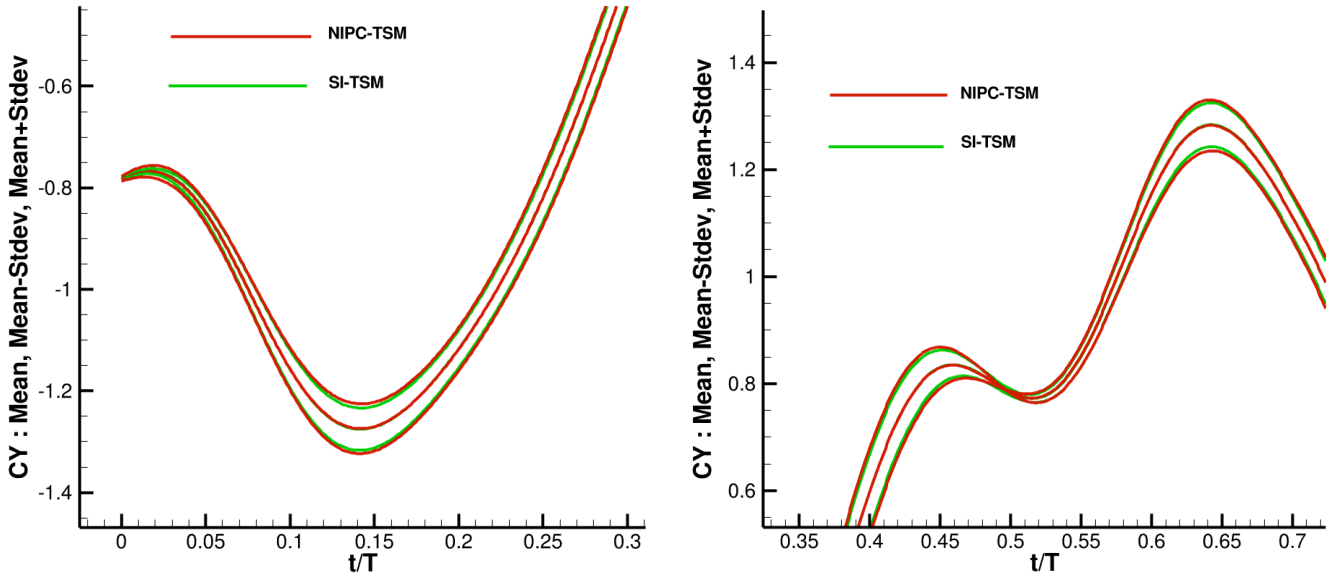

Figure 8: Time evolution of $\overline{C_Y}(t)$, $\overline{C_Y}(t) \pm \sqrt{\sigma(C_Y)(t)}$ over a flow period, computed with NIPC-TSM and SI-TSM. Detailed comparison around minimum (left) and maximum (right) levels.

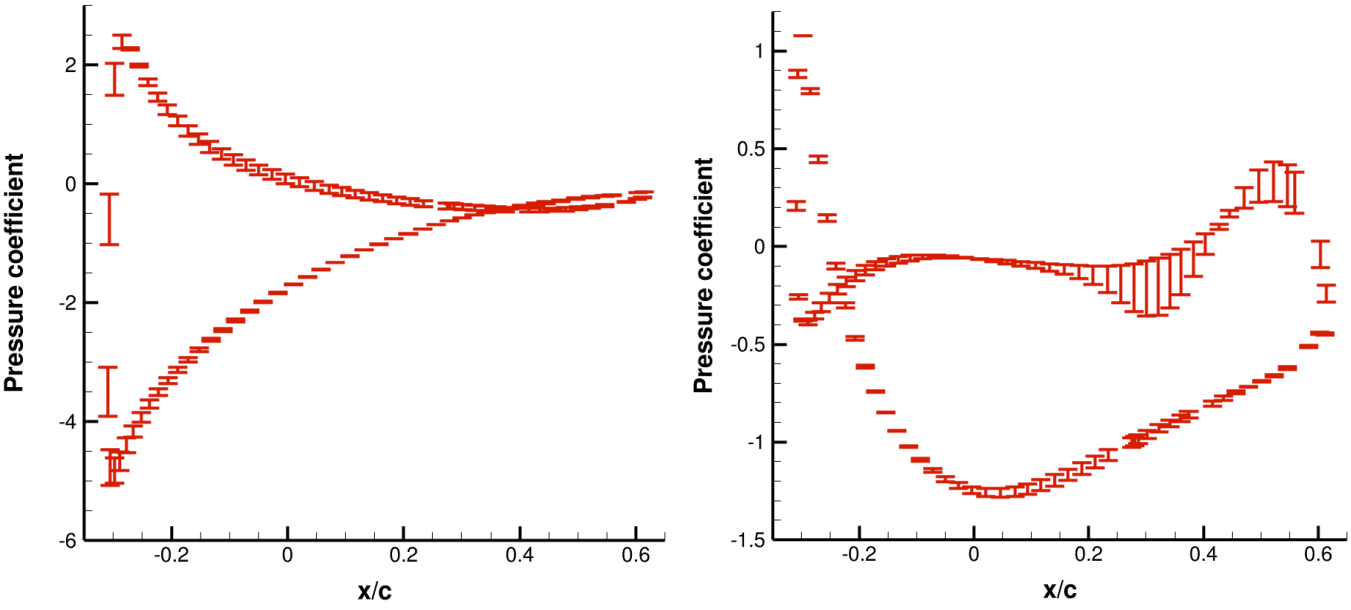

Figure 9: Instantaneous mean pressure distribution and error bar computed at $t/T = 0.25$ and $t/T = 0.5$ using SI-TSM ($n_{prob} = 5$, $n_{TSM} = 17$).

[8] O.P. Le Maître, O.M. Knio, H.N. Najm, R.G. Ghanem. A stochastic projection method for fluid flow: I. Basic Formulation. *Journal of Computational Physics*, 173(2):481-511, 2001.

[9] O.P. Le Maître, M.T. Reagan, H.N. Najm, R.G. Ghanem, O.M. Knio. A stochastic projection method for fluid flow: II. Random process. *Journal of Computational Physics*, 181(1):9-44, 2002.

[10] M.T. Reagan, H.N. Najm, R.G. Ghanem, O.M. Knio. Uncertainty quantification in reacting-flow simulations through non-intrusive spectral projection. *Combustion and Flame*, 132:545-555, 2003.

[11] X. Wan, G. E. Karniadakis. An adaptative multi-element generalized polynomial chaos method for

stochastic differential equations. *Journal of Computational Physics*, 209(2):617Ð642, 2005.

[12] R. Abgrall, P.M. Congedo, S. Galéra. A semi-intrusive deterministic approach to uncertainty quantifications in non-linear fluid flow problems. *INRIA Report n° 7820*, 2011.

[13] R. Abgrall, P.M. Congedo, C. Corre, S. Galéra. A simple semi-intrusive method for uncertainty quantification of shocked flows, comparison with a non-intrusive polynomial chaos method. in *ECCOMAS CFD 2010, J.C.F. Pereira and A. Sequeira (Eds), Lisbon, Portugal*, 2010.

[14] K.C. Hall, J.P. Thomas, W.S. Clark. Computation of Unsteady Nonlinear Flows in Cascades using a Harmonic Balance Technique. *AIAA Journal*, 40(5):879-886, 2002.

[15] A. Gopinath, A. Jameson. Time Spectral Method for Periodic Unsteady Computations Over Two- and Three-Dimensional Bodies. *43rd AIAA Aerospace Sciences Meeting and Exhibit*, AIAA Paper 2005-1220, January 2005.

[16] E. van der Weide, A. Gopinath, A. Jameson. Turbomachinery Applications with the Time Spectral Method. *35th AIAA Fluid Dynamics Conference and Exhibit*, AIAA Paper 2005-4905, June 2005.

[17] K. Ekici, K.C. Hall. Nonlinear Analysis of Unsteady Flows in Multistage Turbomachines Using Harmonic Balance. *AIAA Journal*, 45(5): 1047-1057, 2007.

[18] F. Sicot, G. Puigt, M. Montagnac. Block-Jacobi Implicit Algorithms for the Time Spectral Method. *AIAA Journal*, 46(12):3080Ð3089, 2008.

[19] M.A. Woodgate, K.J. Badcock. Implicit Harmonic Balance Solver for Transonic Flow with Forced Motions. *AIAA Journal*, 47(4):893Ð901, 2009.

[20] X. Su, X. Yuan. Implicit Solution of Time Spectral Method for Periodic Unsteady Flows. *International Journal for Numerical Methods in Fluids*, 63(7):860-876, 2010.

[21] S. Antheaume, C. Corre. Implicit Time Spectral Method for Periodic Incompressible Flows. *AIAA Journal*, 49:791-805, 2011.

[22] M. Baudin, J.M. Martinez. Polynômes de Chaos sous Scilab via la librairie NISP. *42èmes Journées de Statistique*, 2010.

[23] T. Crestaux, O. Le Maître, J.M. Martinez. Polynomial chaos expansion for sensitivity analysis. *Reliability Engineering and System Safety*, 94:1161-1172, 2009.

[24] A.J. Chorin. A numerical method for solving incompressible viscous flow problems. *Journal of Computational Physics*, 2:12-26 (1967).

[25] X. Du, C. Corre, A. Lerat. A third-order finite-volume residual-based scheme for the 2D Euler equations on unstructured grids. *Journal of Computational Physics*, 230:4201-4215, 2011.

[26] B. Koobus, C. Farhat. Second-order time-accurate and geometrically conservative implicit schemes for flow computations on unstructured dynamic meshes. *Comput. Methods Appl. Mech. Engrg.*, 170:103-129, 1999.

[27] T. Kloczko, C. Corre, A. Beccantini. Low-cost implicit schemes for all-speed flows on unstructured meshes. *International Journal for Numerical Methods in Fluids*, 58(5):493-526, 2008.